Inductor Optimization for Active Cell Balancing using Geometric Programming

Matthias Kauer[1], Swaminathan Narayanaswamy[1], Martin Lukasiewycz[1], Sebastian Steinhorst[1], Samarjit Chakraborty[2]
[1] TUM CREATE, Singapore, Email: matthias.kauer@tum-create.edu.sg [2] TU Munich, Germany, Email: samarjit@tum.de

***Abstract*—This paper proposes an optimization methodology for inductor components in active cell balancing architectures of electric vehicle battery packs. For this purpose, we introduce a new mathematical model to quantitatively describe the charge transfer of a family of inductor-based circuits. Utilizing worst case assumptions, this model yields a nonlinear program for designing the inductor and selecting the transfer current. In the next step, we transform this problem into a geometric program that can be efficiently solved. The optimized inductor reduces energy dissipation by at least 20% in various scenarios compared to a previous approach which selected an optimal off-the-shelf inductor.**

I. Introduction and Related Work

Lithium-Ion (Li-Ion) battery cells are utilized in almost all high power Electrical Energy Storage (EES) applications, e.g., Electric Vehicles (EVs). Their operation parameters are quite narrowly specified, but compliance is safety-critical. The cells are thus constantly managed by a Battery Management System (BMS). Since the weakest cell determines the overall capacity of the battery pack in high-voltage series topologies, one main BMS function is cell balancing [1]. The efficiency of the battery pack (and thus, e.g., the driving range of an EV) can be vastly improved by actively transferring charge between cells. Inductor-based charge transfer circuits are more efficient here than those with capacitors and require less volume than transformer architectures [2],[3]. Their performance strongly depends upon the parameters of the circuit itself as evidenced by a discrete optimization that searched commercially available components [4]. Encouraged by these results, we are interested in the design of components specifically for the purpose of cell balancing. Here, we look at the inductor design since it has the strongest impact on performance while other components, mainly the transistors, are far more complex to modify. In our case study (Section IV), we demonstrate that specifically designed inductors reduce the energy dissipation significantly compared to selecting an off-the-shelf inductor [4].

Contributions. The value of this paper is two-fold:
(1) We propose a new mathematical charge transfer model (Section II). It performs on par – regarding precision and computation speed – with existing models, but it greatly facilitates further analytic treatment due to its simplicity.
(2) Using the proposed model to look for the most energy-efficient inductor entails a nonlinear program at first (Section III-B). For a more robust design that produces an inductor which performs well under various situations, we reformulated this program in the Geometric Programming (GP) framework and thereby dramatically improved the solution speed (Section III-C). The inductors designed in this way are at least 20% more energy efficient than the commercial components found in [4] (see case study in Section IV).

This work was financially supported in part by the Singapore National Research Foundation under its Campus for Research Excellence And Technological Enterprise (CREATE) programme.

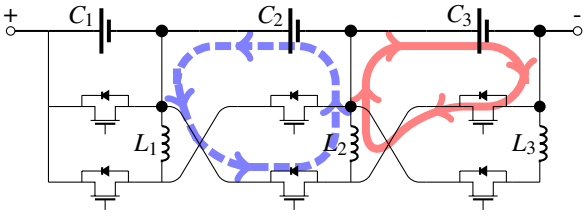

Fig. 1: *In a battery pack with series-connected cells, we equalize Cells C_2 and C_3. In a round-robin fashion, we charge their common inductor L_2 from C_2 and discharge it into C_3 by suitably switching the MOSFETs that control the current flow.*

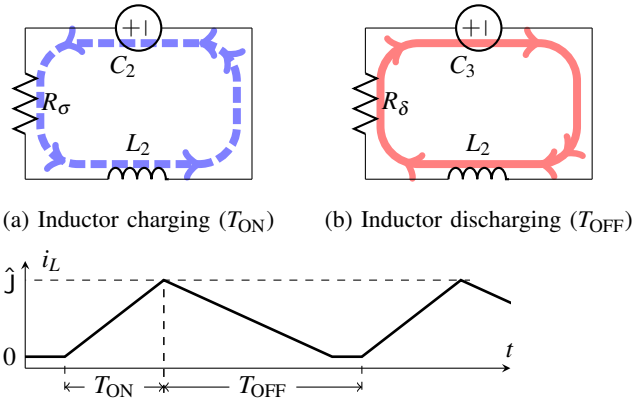

(a) Inductor charging (T_{ON}) (b) Inductor discharging (T_{OFF})

(c) Inductor current i_L

Fig. 2: *By aggregating the resistances on the current path, we can describe the charge transfer in two equivalent circuits, (a) and (b). The current in the inductor rises during T_{ON} until the desired peak value $\hat{\jmath}$ is reached. We then switch the MOSFETs and the inductor discharges during T_{OFF}.*

II. Mathematical Model

Inductor-based charge transfer circuits such as the one from Fig. 1 are driven by a Pulse Width Modulation (PWM) signal. This naturally separates the circuit into two phases: inductor charging (T_{ON}) and inductor discharging phase (T_{OFF}) (cf. Fig. 2; more detail on the low-level MOSFET control in [3]). The charge transfer can subsequently be modeled individually by equivalent circuits (Section II-A). This yields the transfer losses. In addition, we need to account for the switching losses in the MOSFETs that drive the PWM signal (Section II-B).

A. Transfer losses during each PWM step

We can add up the resistances on the active circuit paths and obtain R^σ and R^δ for charging (T_{ON}) and discharging (T_{OFF}) phase, respectively. Such a calculation has been performed, e.g., in [3]. For the general approach described here, it suffices to separate the constant part R_0 from the inductor resistance R_L which is considered a design parameter and remains identical in both phases:

$$R^\sigma = R_0^\sigma + R_L \qquad R^\delta = R_0^\delta + R_L \tag{1}$$

Equivalent circuit. Once the equivalent resistances are established, we can subsequently focus entirely on the equivalent circuit models from Fig. 2. In this work, we aim for a simple quantitative model that enables the application of mathematical optimization techniques. We thus assume that the cell voltage remains constant during individual PWM cycles. This is justified because the overall variation of the cell voltage is small (see Fig. 3) while the frequency of the PWM is high (1kHz to 100kHz). Under these circumstances, both charging (T_{ON}) and discharging (T_{OFF}) phase are governed by the following first-order Ordinary Differential Equation (ODE) where all parameters, particularly i_0 and V, need to be adjusted according to the

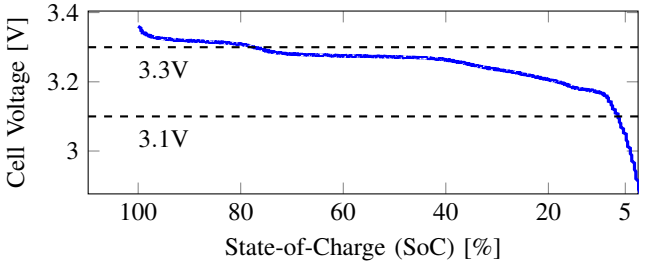

Fig. 3: *We discharged a* 1.1A h *18650 Li-Ion cell from* A123 *Systems with a constant current of* 100mA. *The measured voltage – considered to be the OCV under the modest load – remains within a small range of* 200mV *over the majority of the discharge cycle.*

individual phase.

$$L\frac{\mathrm{d}}{\mathrm{d}t}i(t)+Ri(t)=V \qquad i(t)=i_0 \tag{2}$$

The unique solution of (2) is given by

$$i(t,V,i_0,R)=\frac{V}{R}-\frac{V-i_0R}{R}\exp\Big(\frac{-R}{L}t\Big). \tag{3}$$

We are mainly interested in the amount of charge that is transferred over a certain time T. This quantity can be calculated by integrating current $i(t)$ from (3):

$$q(T,V,i_0,R)=\frac{V}{R}T+\frac{L(V-i_0R)}{R^2}\left[\exp\Big(\frac{-R}{L}T\Big)-1\right] \tag{4}$$

Here, the integration constant is chosen such that $q(0)=0$.

Timing. To obtain the charge evolution corresponding to an entire PWM cycle, we need to evaluate (4) for the two phases depicted in Fig. 2. Toward this, note that $i(t)$ from (3) is invertible and we can obtain a desired current i_d after a period of T_d given by:

$$T_d(i_d,V,i_0,R)=\frac{-L}{R}\log\Big(\frac{V-i_dR}{V-i_0R}\Big) \tag{5}$$

For the purpose of implementation and easier analysis, we substitute (5) into the equation for the transferred charge (4). This yields the following closed-form solution.

$$\begin{aligned}q_d(i_d,V,i_0,R)=&\frac{V}{R}T_d(i_d)+\frac{L(V-i_0R)}{R^2}\Big[\frac{V-i_dR}{V-i_0R}-1\Big]\\=&\frac{-LV}{R^2}\log\Big(\frac{V-i_dR}{V-i_0R}\Big)+\frac{L(i_0-i_d)}{R}\end{aligned} \tag{6}$$

We design T_{ON} such that the inductor reaches the desired current $\hat{\mathrm{J}}$ at its end. During T_{OFF}, we ensure that there remains no current in the inductor ($i_d=0$). Overall, we are thus working with $[V \quad R \quad i_d \quad i_0]$ given by $\left[V^\sigma \quad R^\sigma \quad \hat{\mathrm{J}} \quad 0\right]$ and $\left[-V^\delta \quad R^\delta \quad 0 \quad \hat{\mathrm{J}}\right]$ during T_{ON} and T_{OFF}, respectively.

With this knowledge, we can individually derive q_d from (6) for both T_{ON} as well as T_{OFF} case with respect to V. Using (7), this shows that q_d decreases with $|V|$ for both phases:

$$\begin{aligned}\frac{\mathrm{d}}{\mathrm{d}V}V\log\big(\frac{V-R\hat{\mathrm{J}}}{V}\big)=&\log\big(1-\frac{R\hat{\mathrm{J}}}{V}\big)+V\frac{V}{V-R\hat{\mathrm{J}}}\cdot\frac{V-(V-R\hat{\mathrm{J}})}{V^2}\\\geq&\frac{R\hat{\mathrm{J}}}{V}\Big/\frac{V-R\hat{\mathrm{J}}}{V}+\frac{V-R\hat{\mathrm{J}}}{V^2}=0\end{aligned} \tag{7}$$

The inequality holds since $\log(1+v)\geq\frac{v}{1+v}\quad\forall v>-1$.

Bounding charge transfer. Over multiple PWM cycles, the transferred charge evolves only according to the involved cell voltages that follow the changes in State-of-Charge (SoC). Cell voltage increases monotonously with SoC, however. Therefore, the initial voltages of sender, V_0^σ, and receiver, V_0^δ, are the highest and lowest voltages to be considered. With this in mind and since q_d from (6) decreases with $|V|$ (see (7)), we can bound the transferred charge:

$$q_d(V)\geq q_{\min}:=q_d(V_0^\sigma),\qquad q_d(V)\leq q_{\max}:=q_d(V_0^\delta) \tag{8}$$

In other words, the *most charge* is taken from the transmitting cell or put into the receiving cell if they were to hypothetically reach V_0^δ, the initial voltage of the receiver. Conversely, the *least charge* leaves the transmitter or reaches the receiving cell if either were to measure V_0^σ, the initial voltage of the transmitter. Since the voltage evolves so slowly with SoC (see Fig. 3), these bounds are quite tight. For evaluation, we assume circuit parameters $\left[R \quad L \quad \hat{\mathrm{J}} \quad V_0^\delta \quad V_0^\sigma\right]=[0.25 \quad 1\text{e-}4 \quad 1.0 \quad 3.1\mathrm{V} \quad 3.3\mathrm{V}]$. This scenario is highly unfavorable for the precision due to the high resistance and the unrealistically large voltage gap (roughly corresponding to SoCs of 5% and 80%). Nevertheless, the worst case relative error remains small with $\frac{|q_d(V_0^\delta)-q_d(V_0^\sigma)|}{|q_d(V_0^\delta)|}\leq 6.8\%$.

Bounding transfer losses. Given a relation $q\to V(q)$, we can calculate the stored energy of a cell as $E_{\mathrm{batt}}(Q)=\int_0^Q V(q)dq$. The energy that is lost during the transfer in a single PWM cycle is thus given by

$$\begin{aligned}E_{tf}=&E_{\mathrm{batt}}(Q^\sigma)-E_{\mathrm{batt}}(Q^\sigma-q^\sigma)-\left[E_{\mathrm{batt}}(Q^\delta+q^\delta)-E_{\mathrm{batt}}(Q^\delta)\right]\\=&\int_{Q^\sigma-q^\sigma}^{Q^\sigma}V(q)dq-\int_{Q^\delta}^{Q^\delta+q^\delta}V(q)dq\leq V_0^\sigma q^\sigma-V_0^\delta q^\delta.\end{aligned} \tag{9}$$

B. Switching losses during each PWM step

The switching of a MOSFET dissipates energy due to charging and discharging of input and output capacitances of the transistor in every PWM cycle. This loss is given by $\frac{1}{2}C_{OSS}V_{ds}^2$ where C_{OSS} and V_{ds} are output capacitance and drain-source voltage of the transistor, respectively. In addition, the current that is drawn during t_{ON} – summarizing turn-on delay and rise time – and t_{OFF} – consisting of turn-off delay and fall time – cannot be utilized. This entails losses of the form $\frac{1}{2}tI_{ds}V_{ds}$ where I_{ds} is the drain-source current of the transistor. Please refer to Chapter 4.3 "Switching Losses" in [5] for further information.

Since all the involved voltages are upper-bounded by V_0^σ and I_{ds} vanishes at the beginning of T_{ON} as well as at the end of T_{OFF}, the switching losses for every single PWM cycle can be characterized by (10).

$$E_{sw}=\frac{1}{2}(t_{\mathrm{OFF}}+t_{\mathrm{ON}})\hat{\mathrm{J}}V_0^\sigma+C_{OSS}V_\sigma^2 \tag{10}$$

III. Optimal Inductor Design

In this section, we aim to find the optimal inductor for any of the inductor-based charge transfer architectures that can be described by the mathematical model presented in Section II, e.g., the architectures from [2], [3]. The objective is to minimize the average energy losses for a set $\mathscr{S}$ of scenarios $s=\left[V^\sigma \quad V^\delta\right]$.

A. Inductor Design Constraint

In order to minimize transfer (Section II-A) and switching (Section II-B) losses, we would like to have an inductor with microscopic resistance and large inductance that supports gigantic peak currents. However, there is obviously a trade-off involved between these features. Using the procedure described in Chapter 14 "Inductor Design" of [5], we begin by ensuring that the following inequality holds.

$$K_g\geq\frac{\rho L^2I_{\max}^2}{B_{\max}^2R_LK_u} \tag{11}$$

Here, K_g is the core geometrical constant summarizing the size and the layout of the core. It can be obtained from data tables. $\rho = 1.724\text{e-}6\Omega\text{cm}^{-2}$ is the resistivity of copper wire. $I_{\max}$ can be assumed to be the peak current $\hat{\mathrm{J}}$ for non-dominated designs. K_u is the winding fill factor and is in the range of $K_u = 0.7$. Finally, we set $B_{\max} = 0.3\text{T}$ for most ferrite core materials according to Chapter 9.4.5 "Design of Inductors" in [6].

Given the dimension of the overall circuitry, we select a suitable core which determines the geometrical constant K_g. From any combination of $L, R, \hat{\mathrm{J}}$ that fulfills (11), we can then go back to [5] and calculate air gap length l_g as well as number of turns n. This means that selecting $L, R, \hat{\mathrm{J}}$ *implicitly fixes the entire inductor design*.

B. Nonlinear programming formulation

A straightforward implementation of our design problem is the introduction of variable N for the number of PWM cycles that are required to conclude the balancing in the worst case. We obtain the difference ΔQ from the Open Circuit Voltage (OCV) (see data in Fig. 3). If measuring the OCV is not feasible, ΔQ can be obtained using SoC estimation. The calculation of PWM cycles N assumes that both the charge taken out of the sending cell and the charge arriving in the receiving cell are minimal as given by (8). With $s = \begin{bmatrix} V^\sigma & V^\delta \end{bmatrix}$ referring to individual scenarios, we thus formulate:

$$\begin{aligned} \min \quad & \sum_{s\in\mathscr{S}} N^s \cdot (E^s_{tf} + E^s_{sw}) \quad \text{using (9), (10)} \\ \text{s.t.} \quad & \text{Inductor constraint (11)} \\ & N^s = \frac{\Delta Q^s}{q^{\sigma,s}_{\min} + q^{\delta,s}_{\min}} \\ & N^s \cdot ({T_{\text{ON}}}^s + {T_{\text{OFF}}}^s) \le T_{\max} \quad \forall s \in \mathscr{S} \end{aligned} \tag{12}$$

Mathematical program (12) is based on main variables $R, L, \hat{\mathrm{J}}^s$ and auxiliary variables ${T_{\text{ON}}}^s, {T_{\text{OFF}}}^s, N^s$. Although it is nonlinear, it can be solved, e.g., using a nonlinear Sequential Quadratic Programming (SQP) solver. Notwithstanding, it is unclear whether this approach yields a global or only a local minimum without further analysis, e.g., regarding convexity.

C. Geometric programming formulation

To solve larger problems than the nonlinear formulation from Section III-B allows, we have transformed (12) to conform to the Geometric Programming (GP) framework. After [7], a GP problem in standard form is:

$$\begin{aligned} \min \quad & f_0(x) \\ \text{s.t.} \quad & f_i(x) \le 1 \quad \forall i = 1,\dots,m \\ & g_i(x) = 1 \quad \forall i = 1,\dots,p \end{aligned}$$

where $x = [x_1,\dots,x_n]$ is a vector of positive real-valued decision variables. f_i and g_i are posynomial and monomial functions, respectively. A monomial has the form:

$$m(x) = c x_1^{a_1} x_2^{a_2} \dots x_n^{a_n} \qquad c > 0, a_i \in \mathbb{R}$$

Posynomials are sums of monomials and closed under addition, multiplication, positive scaling as well as division by monomials. Geometric Programming (GP) is a special form of convex optimization. GPs have polynomial time computational complexity and can be solved very efficiently by a variety of off-the-shelf solvers.

In the following, we will mainly use the power series version of the natural logarithm given in (13) to transform (12).

$$\log(1+z) = z - \frac{z^2}{2} + \frac{z^3}{3} + \dots \tag{13}$$

Charge transfer reformulation. Starting from (6) describing q_d, the charge transferred during a PWM cycle, we can transform $q^\sigma_{\max}$ from (8) as follows.

$$\begin{aligned} q^\sigma_{\max} =& \frac{-LV_0^\delta}{R^{\sigma 2}} \log\Big(1 - \frac{\hat{\mathrm{J}} R^\sigma}{V_0^\delta}\Big) - \frac{L\hat{\mathrm{J}}}{R^\sigma} \\ \approx& \frac{LV_0^\delta}{R^{\sigma 2}} \Big[\frac{\hat{\mathrm{J}} R^\sigma}{V_0^\delta} + \frac{1}{2}\Big(\frac{\hat{\mathrm{J}} R^\sigma}{V_0^\delta}\Big)^2 + \frac{1}{3}\Big(\frac{\hat{\mathrm{J}} R^\sigma}{V_0^\delta}\Big)^3\Big] - \frac{L\hat{\mathrm{J}}}{R^\sigma} \\ =& \frac{L\hat{\mathrm{J}}^2}{2V_0^\delta} + \frac{L\hat{\mathrm{J}}^3 R^\sigma}{3V_0^{\delta 2}} \end{aligned} \tag{14}$$

Using relation $\log(\frac{1}{v}) = -\log(v)$ for $q^\delta_{\min}$, we obtain

$$\begin{aligned} q^\delta_{\min} =& \frac{-L(-V_0^\sigma)}{R^{\delta 2}} \log\Big(\frac{-V_0^\sigma}{-V_0^\sigma - \hat{\mathrm{J}} R^\delta}\Big) + \frac{L\hat{\mathrm{J}}}{R^\delta} \\ \approx& \frac{L\hat{\mathrm{J}}^2}{2V_0^\sigma} - \frac{L\hat{\mathrm{J}}^3 R^\delta}{3V^{\sigma 2}}. \end{aligned} \tag{15}$$

PWM Cycle calculation. The number of PWM cycles, N, can be bounded from below by

$$N \ge \frac{\Delta Q}{q^\sigma_{\min} + q^\delta_{\min}}. \tag{16}$$

This can be reformulated to

$$\begin{aligned} \frac{\Delta Q}{N} \le& q^\sigma_{\min} + q^\delta_{\min} = \frac{L\hat{\mathrm{J}}^2}{2V_0^\delta} + \frac{L\hat{\mathrm{J}}^3 R^\sigma}{3V_0^{\delta 2}} + \frac{L\hat{\mathrm{J}}^2}{2V_0^\delta} - \frac{L\hat{\mathrm{J}}^3 R^\delta}{3V_0^{\delta 2}} \\ =& \frac{L\hat{\mathrm{J}}^2}{V_0^\delta} + \frac{L\hat{\mathrm{J}}^3 \big(R_c^\sigma + R_L - R_c^\delta - R_L\big)}{3V_0^{\delta 2}}. \end{aligned}$$

We thus arrive at a posynomial formulation:

$$\frac{\Delta Q}{N} + \max\left\{0, \frac{L\hat{\mathrm{J}}^3 (R_c^\delta - R_c^\sigma)}{3V^{\delta 2}}\right\} \le \frac{L\hat{\mathrm{J}}^2}{V^\delta} \tag{17}$$

Here, the max operation can and must be evaluated a priori since the resistances of the remaining circuit without the inductor, R_c^σ, R_c^δ, are constant from the perspective of this optimization.

Switching loss estimation. Formulation (10) for the switching losses is already a posynomial in R^σ, R^δ, $\hat{\mathrm{J}}$, V^σ.

Transfer loss calculation. Equation (9) that describes the transfer losses is a posynomial in R^σ, R^δ, $\hat{\mathrm{J}}$, L if we employ (14) and (15) for the charge transfer. This can be seen in the following.

$$\begin{aligned} E_{tf} =& V_0^\sigma \cdot q^\sigma_{\max} - V_0^\delta \cdot q^\delta_{\min} \\ =& V_0^\sigma \big(\frac{L\hat{\mathrm{J}}^2}{2V_0^\delta} + \frac{L\hat{\mathrm{J}}^3 R^\sigma}{3V_0^{\delta 2}}\big) - V_0^\delta \big(\frac{L\hat{\mathrm{J}}^2}{2V_0^\sigma} - \frac{L\hat{\mathrm{J}}^3 R^\delta}{3V_0^{\sigma 2}}\big) \\ =& \frac{L\hat{\mathrm{J}}^2}{2} \big(\underbrace{\frac{V_0^\sigma}{V_0^\delta} - \frac{V_0^\delta}{V_0^\sigma}}_{\ge 0}\big) + \frac{L\hat{\mathrm{J}}^3 R^\sigma V_0^\sigma}{3V_0^{\delta 2}} + \frac{L\hat{\mathrm{J}}^3 R^\delta V_0^\delta}{3V_0^{\sigma 2}} \end{aligned} \tag{18}$$

Timing estimation. To estimate T_{ON}, we start from (5) and let $i_0 = 0$ as discussed. Using (13), we can then reformulate this as follows.

$$\begin{aligned} T_{\text{ON}} =& \frac{-L}{R^\sigma} \log\Big(1 - \frac{\hat{\mathrm{J}} R^\sigma}{V^\sigma}\Big) \\ \approx& \frac{L\hat{\mathrm{J}}}{V^\sigma} + \frac{L\hat{\mathrm{J}}^2 R^\sigma}{2V^{\sigma 2}} + \frac{L\hat{\mathrm{J}}^3 R^{\sigma 2}}{V^{\sigma 3}} \end{aligned} \tag{19}$$

Equation (19) is a posynomial in the variables $R^\sigma, L, \hat{\mathrm{J}}$ and even

V^σ. Performing the identical transformation for T_{OFF} does not lead to a posynomial in the same way, however. We therefore utilize only the first term in the power series representation and thus obtain an upper bound:

$$T_{\text{OFF}} = \frac{L}{R^\delta} \log\left(1 + \frac{\hat{J} R^\delta}{V^\delta}\right) \leq \frac{L\hat{J}}{V^\delta} \tag{20}$$

Here, the relation $\log(\frac{1}{v}) = -\log(v)$ was used in the first equality. In total, if we want to ensure that the duration of an entire balancing run remains below a threshold $T_{\max}$, we can thus utilize the following constraint.

$$T_{\text{ON}} + T_{\text{OFF}} \leq \frac{L\hat{J}}{V^\delta} + \frac{L\hat{J}}{V^\sigma} + \frac{L\hat{J}^2 R^\sigma}{2V^{\sigma 2}} + \frac{L\hat{J}^3 R^{\sigma 2}}{V^{\sigma 3}} \leq \frac{T_{\max}}{N} \tag{21}$$

Here, only the second inequality is part of the optimization. Since its left-hand side is a posynomial and its right-hand side a monomial, it is compatible with the GP approach.

Overall problem. With the help of the posynomial reformulations that were just discussed, we can now rewrite problem (12) in the GP paradigm:

$$\begin{aligned} \min \quad & \sum_{s\in\mathscr{S}} N^s \cdot (E^s_{tf} + E^s_{sw}) \quad \text{using (10), (18)} \\ \text{s.t.} \quad & \text{Inductor constraint (11)} \quad \forall \hat{J}^s \\ & \text{Cycle count constraint (17)} \quad \forall N^s \\ & \text{Time constraint (21)} \quad \forall T_{\text{ON}}{}^s, T_{\text{OFF}}{}^s, N^s \end{aligned} \tag{22}$$

To solve problem (22) we used CVX, a MATLAB package that suitably reformulates geometric programs to equivalent convex representations and solves them [8].

IV. Case Study

In this section, we evaluate the scalability of the proposed approach as well as the performance of the resulting inductors.

Design quality. For a demonstration of how the optimization is used in practice, we start from a design using off-the-shelf components that was considered optimal by the search algorithm of [4] for the same circuit architecture. It uses the MURATA(8.2) inductor with effective volume $V_e = 893\text{mm}^3$ and the ONSEMI(7.8) MOSFET. This entails the following circuit parameters.

$$\begin{bmatrix} R_0^\sigma & R_0^\delta & \star \\ C_{OSS} & t_{ON} & t_{OFF} \end{bmatrix} = \begin{bmatrix} 35\text{m}\Omega & 35\text{m}\Omega & \star \\ 125\text{pF} & 44\text{ns} & 168\text{ns} \end{bmatrix} \tag{23}$$

We base our designs on cores POT1107 and ETD29, as described, e.g., by the data tables in Appendix D of [5]. POT1107 has geometric constrant $K_g = 6.67\text{e-}4$ and effective volume $V_e = 251\text{mm}^3$ and should lead to a final product with volume in the range of the MURATA(8.2). The larger ETD29 with $K_g = 9.78\text{e-}2$ and $V_e = 5470\text{mm}^3$ is included for comparison. Volume data has been obtained from the corresponding part numbers 0R42929EC and 0F41107UG in the Magnetics catalog.

The scenarios we take into consideration are chosen such that both cells remain within a typical SoC range of $[10\%, 90\%]$ with a maximum difference of 10 percentage points. They are detailed in Table I.

Scenario	s_1	s_2	s_3	s_4	s_5
$\text{SoC}^\sigma(V^\sigma)$	0.9(3.315V)	0.76(3.284V)	0.55(3.273V)	0.41(3.262V)	0.25(3.220V)
$\text{SoC}^\delta(V^\delta)$	0.82(3.304V)	0.72(3.279V)	0.49(3.271V)	0.33(3.240V)	0.18(3.197V)
ΔQ[C]	316.5	172.8	189.2	300.2	287.8

TABLE I: *Scenarios for inductor design*

# Scenarios $\lvert\mathscr{S}\rvert$	1	5	10	50	100
Runtime [s]	2.45	9.33	15.36	82.14	179.97

TABLE II: *Runtime measurements for growing scenario vector*

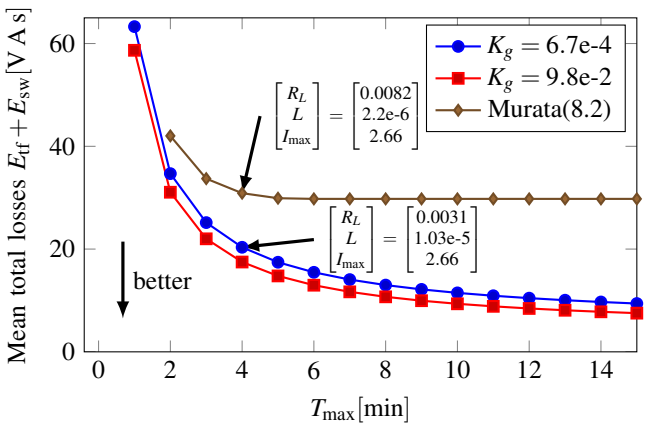

Fig. 4: *Specifically designing the inductor reduces the average energy losses for the scenarios in Table I of a fixed inductor at least by 20%.*

Fig. 4 shows the results of our experiment. Each of the marks represents an inductor design that is optimal for a certain allotted balancing time $T_{\max}$ and core with geometrical constant K_g. All the curves flatten out once $T_{\max}$ is so large that time constraint (21) is not active in the optimization any longer. For $T_{\max} = 1\text{min}$, the required current is too large for the fixed inductor. Otherwise, the comparable designs from the proposed approach dissipate at least 20% less energy ($\frac{42\text{V A s}}{34.7\text{V A s}} = 1.21$ for $T_{\max} = 2\text{min}$). The larger core yields only mediocre further benefits.

Furthermore, we have evaluated the relative errors that arise from bounding the charge transfer in (8) as well as from the power series reformulations (14) and (15). Both remain well under 1% in the optimal points of GP problem (22).

Scalability. To measure the performance of GP instance (22) we select the scenarios randomly by drawing voltage pairs according to $V \sim \mathscr{N}(3.15, 0.1)$, using the larger one as sender and calculating ΔQ via Fig. 3. We solve GP instance (22) with increasing $\lvert\mathscr{S}\rvert$ and record the required runtime. This procedure yields Table II. Clearly, the scalability is excellent – almost linear – probably because the GP formulation is quite sparse. Even larger problems are solved in merely minutes on the computer we utilized (Intel i5-2540M @ 2.60GHz with 8GB RAM).

V. Concluding Remarks

We presented a new mathematical model to quantify inductor-based charge transfer circuits that leads to a geometric program for parameter optimization. By specifically designing the inductor in this way, we were able to significantly improve the energy efficiency during balancing compared to off-the-shelf components.

References

[1] S. Moore and P. Schneider, "A Review of Cell Equalization Methods for Lithium Ion and Lithium Polymer Battery Systems," *SAE Technical Paper Series*, 2001.

[2] N. H. Kutkut, "A Modular Nondissipative Current Diverter for EV Battery Charge Equalization," in *Proc. of APEC*, 1998.

[3] M. Kauer, S. Naranayaswami, S. Steinhorst, M. Lukasiewycz, S. Chakraborty, and L. Hedrich, "Modular System-Level Architecture for Concurrent Cell Balancing," in *Proc. of DAC*, 2013.

[4] S. Narayanaswamy, S. Steinhorst, M. Lukasiewycz, M. Kauer, and S. Chakraborty, "Optimal Dimensioning of Active Cell Balancing Architectures," in *Proc. of DATE*, 2014.

[5] R. W. Erickson and D. Maksimovic, *Fundamentals of Power Electronics*. Springer, 2001.

[6] R. Kories and H. Schmidt-Walter, *Electrical Engineering: A Pocket Reference*. Springer, 2003.

[7] S. Boyd, S.-J. Kim, L. Vandenberghe, and A. Hassibi, "A Tutorial on Geometric Programming," *Optimization and engineering*, vol. 8, no. 1, pp. 67–127, 2007.

[8] M. Grant and S. Boyd, "CVX: Matlab Software for Disciplined Convex Programming, version 2.1," http://cvxr.com/cvx, Mar. 2014.